Pleiotropic activity of systemically delivered angiogenin in the SOD1

AUTHOR(S)

Martin Crivello, Saidhbhe L. O'Riordan, Ina Woods, Sarah Cannon, Luise Halang, Karen S. Coughlan, Marion C. Hogg, Sebastian A. Lewandowski, Jochen HM Prehn

CITATION

Crivello, Martin; O'Riordan, Saidhbhe L.; Woods, Ina; Cannon, Sarah; Halang, Luise; Coughlan, Karen S.; et al. (2018): Pleiotropic activity of systemically delivered angiogenin in the SOD1. figshare. Journal contribution. https://hdl.handle.net/10779/rcsi.10789721.v1

HANDLE

10779/rcsi.10789721.v1

Pleiotropic activity of systemically delivered angiogenin in the SOD1^{G93A} mouse model

Martin Crivello[a], Saidhbhe L. O'Riordan[a], Ina Woods[1], Sarah Cannon[a], Luise Halang[a], Karen S. Coughlan[a], Marion C. Hogg[a], Sebastian A. Lewandowski[b] and Jochen H. M. Prehn[a,CA]

[a]Department of Physiology and Medical Physics, Centre for the Study of Neurological Disorders, Royal College of Surgeons in Ireland, 123 St. Stephen's Green, Dublin 2, Ireland. [b]Tissue Biology Laboratory, Department of Medical Biochemistry and Biophysics, Karolinska Institute, Scheeles v. 2, 17177, Stockholm, Sweden.

Martin Crivello <martincgarcia@rcsi.ie>; Saidhbhe L. O'Riordan < oriordan@caltech.edu>; Ina Woods <ikoegel@rcsi.ie>; Sarah Cannon <sarah.cannon@mu.ie>; Luise Halang <luisehalang@rcsi.ie>; Karen S. Coughlan < karencoughlan@rcsi.ie>; Marion C. Hogg <marionhogg@rcsi.ie>; Sebastian A. Lewandowski <sebastian.lewandowski@ki.se>

[CA] Corresponding author: Prof. Jochen H. M. Prehn, Department of Physiology and Medical Physics, Centre for the Study of Neurological Disorders, Royal College of Surgeons in Ireland, 123 St. Stephen's Green, Dublin 2, Ireland.
Email: prehn@rcsi.ie
Tel: + 353 1 402 2255
Fax: + 353 1 402 2447

Abstract

Loss-of-function mutations in the *angiogenin* (*ANG*) gene have been identified in familial and sporadic ALS patients. Previous work from our group identified human ANG (huANG) to protect motoneurons *in vitro*, and provided proof-of-concept that daily intraperitoneal (i.p.) huANG injections post-symptom onset increased lifespan and delayed disease progression in $SOD1^{G93A}$ mice. huANG's mechanism of action remains less well understood. Here, we implemented a preclinical *in vivo* design to validate our previous results, provide pharmacokinetic and protein distribution data after systemic administration, and explore potential pleiotropic activities of huANG *in vivo*. $SOD1^{G93A}$ mice (n = 45) and non-transgenic controls (n = 31) were sex- age- and litter-matched according to the 2010 European ALS/MND group guidelines, and treated with huANG (1 µg, i.p., 3 times/week) or vehicle from 90 days on. huANG treatment increased survival and delayed motor dysfunction as assessed by rotarod in $SOD1^{G93A}$ mice. Increased huANG serum levels were detectable 2 and 24 h after i.p. injection equally in transgenic and non-transgenic mice. Exogenous huANG localized to spinal cord astrocytes, supporting a glia-mediated, paracrinemechanism of action; uptake into endothelial cells was also observed. 1 µg huANG or vehicle were administered from 90 to 115 days of age for histological analysis. Vehicle-treated $SOD1^{G93A}$ mice showed decreased motoneuron numbers and vascular length per ventral horn area, while huANG treatment resulted in improved vascular network maintenance and motoneuron survival. Our data suggest huANG represents a new class of pleiotropic ALS therapeutic that acts on the spinal cord vasculature and glia to delay motoneuron degeneration and disease progression.

1. Introduction

Amyotrophic lateral sclerosis (ALS) is a progressive neurodegenerative disease characterized by the loss of upper and lower motoneurons, leading to the weakening of limb, respiratory and bulbar muscles. Prognosis is usually poor, with most patients surviving 3–5 years after initial diagnosis (Robberecht and Philips, 2013). Despite recent advances in understanding the genetics and molecular pathophysiology of ALS, the aetiology of the disease is still poorly understood, with limited treatment options and no known cure. Riluzole, capable of extending survival in a subset of patients by a few months, was the only approved treatment for ALS until recently when the antioxidant Edaravone was approved for treating the disease in Japan and the USA (Rothstein, 2017).

Since the realization in the early 1990s that mutations in the Cu/Zn superoxide dismutase-1 (*SOD1*) gene are responsible for some heritable forms of ALS (Rosen, 1993), the list of discovered ALS-related genes has increased steadily. Mutations found in *TARDBP*, *FUS*, *TAF15*, *senataxin* (*SETX*) and *angiogenin* (*ANG*, also known as *ribonuclease A 5*) highlight RNA metabolism defects as key processes in ALS (Robberecht and Philips, 2013). In a previous study we linked loss-of-function mutations in the *ANG* gene to familial and apparently sporadic cases of ALS (Greenway et al., 2006), a finding confirmed in subsequent genetic studies (Van Es et al., 2011; Wu et al., 2007).

While initially identified as an angiogenic factor extracted from human adenocarcinoma cells (Fett et al., 1985), we later demonstrated that ANG is expressed in motoneurons (Greenway et al., 2006) and protects cultured motoneurons against excitotoxic and hypoxic injury (Kieran et al., 2008; Sebastià et al., 2009). Furthermore, we showed that motoneurons secrete ANG during stress conditions, and that secreted ANG is taken by astroglia through clathrin-mediated endocytosis and mediates neuroprotection in paracrine (Skorupa et al., 2012). We also provided in vivo proof-of-concept that daily, systemic administration of human ANG (huANG) protein increases lifespan and delays motor dysfunction in the $SOD1^{G93A}$ mouse model of familial ALS (Kieran et al., 2008). However, ANG's mechanism of action after systemic administration *in vivo* is less well characterized, and could also involve effects on angiogenesis and vascularization. Indeed, previous work demonstrated that ALS-associated huANG variants displayed reduced angiogenic activity, either by a deficiency in its ribonuclease activity, nuclear translocation, or both (Wu et al., 2007).

Finding new therapeutics for ALS remains a top priority in the field. Despite the many advantages of preclinical ALS mouse models, the consistent failure to translate encouraging results into positive clinical outcomes prompted the European ALS/MND group to review past results and release research guidelines (Ludolph et al., 2010). Thus, the aim of this study was to validate our previous *in vivo* proof-of-concept work by adopting these guidelines in a pre-clinical study design, provide pharmacokinetic data on serum levels, determine huANG protein distribution after systemic administration in vivo, and to explore potential pleiotropic activities of huANG *in vivo*.

2. Material and methods

2.1. Animals

SOD1G93A C57B6.Cg-Tg mice ($SOD1^{G93A}$) were purchased from Jackson Laboratory (Bar Harbor, ME, USA). These mice are congenic on the C57Bl6 background and carry a high copy number of the G93A mutant *SOD1* transgene. Mice were genotyped and copy number checked by PCR. Mice were housed in cages of between 3 and 5 mice and all mice for this study were age-, gender- and litter-matched according to ALS pre-clinical trial guidelines (Ludolph et al., 2010). Mice were housed at constant temperature (22 °C) on a 12 h light/dark cycle (07:00 h on, 19:00 h off), with *ad libitum* food and water available. All experiments were carried out under license (AE19127/P004) from the Health Products Regulatory Authority, Ireland, with ethical approval from the Royal College of Surgeons in Ireland Research Ethics Committee (REC1122b).

2.2. In vivo huANG treatments

Recombinant huANG (265AN250/CF, R&D Systems) stock was dissolved in sterile PBS (vehicle). $SOD1^{G93A}$ mice and their wild-type (WT) counterparts were given huANG (1 µg i.p. injection, 3 times a week) or vehicle from PND 90 until PND 115 (Fig. 1a; for histological studies) or until end stage of disease (Fig. 1b; survival and motor function studies). Exact numbers are detailed in Supplementary material 1 and 2. Weight was measured twice weekly and is summarized in Supplemental material 3. End stage of ALS disease progression was determined by the extreme weakening or loss of hind limb function and loss of righting reflex within 30 s after the mice were placed on their back (Ludolph et al., 2010). The triweekly 1 µg huANG dosage was chosen after analysis of cost concerns following a daily dosage study by our lab (Kieran et al., 2008) and after a previous dose-response pilot study in SOD1G93A mice did not reveal an improvement on survival or motor function in mice treated with 10 µg huANG versus the lower dosage.

2.3. Serum analysis of huANG levels after systemic protein injection

A single i.p. injection of 1 µg huANG or vehicle was given at PND 90 (exact animal numbers detailed in Supplementary material 4) and blood samples collected via cardiac puncture after 0, 2 and 24 h. Whole blood was collected from each subject in sterile 1.5 mL polypropylene tubes by applying a small amount of negative pressure into the heart with a 26-gauge needle (to avoid rupture of erythrocytes) and allowed to coagulate at room temperature for 15–30 min. Serum was then extracted by 10 min centrifugation at 1000-2000xg and analysed for huANG content by ELISA kit (DAN00, R&D Systems) following the manufacturer's protocol. Briefly, the colorimetric output of the assay was quantified using a Multiskan EX photometer (Thermo Scientific) by reading the optical density of each sample and standard at 450 nm. Values from a second reading at 570 nm were subtracted from the 450 nm readings as recommended by the manufacturer to correct for plate imperfections. Haemolysis of samples was primarily assessed on a visual basis and haemolysed samples were subsequently eliminated after spectrophotometric measurement at 540 nM. A standard curve was generated on the same plate using the provided standards of known huANG protein concentration.

2.4. Assessment of lifespan and disease progression in vivo

huANG (1 μg) was administered via i.p. injection 3 times weekly (due to bioavailability calculated in PK/PD studies). For lifespan and motor function assessment, animals were age-, gender- and litter-matched in accordance with recent ALS guidelines for the generation of preclinical data (Ludolph et al., 2010). Mice underwent one week of training before experimental measurements. Tests were performed blinded by a single observer. Motor function was tested in all mice by rotarod (Stoelting, Illinois, USA) twice weekly. Latency to fall was assessed up to three times per mouse per session for a maximum of 180 s and last value recorded (Gurney et al., 1994).

2.5. Tissue collection for vascular structure staining

Following ethical guidelines, mice were terminally anesthetised and transcardially perfused with PBS at a slow rate (approx. 10 mL/min) until no blood remained and organs turned a pale colour. Spinal cords (L1-L5) were removed and fixed with PFA 4% for 1 h and then transferred to 30% sucrose for cryoprotection for 1–2 days. The tissues were then cut with the cryostat into 16 μm sections and mounted on Superfrost plus slides (MNJ-700-010N, VWR).

2.6. Vasculature imaging and stereological analysis

The neurovascular unit is composed of endothelial cells, contractile cells expressing α-smooth muscle actin (ASMA)—namely smooth muscle cells (SMCs) and pericytes—and astrocyte processes (Attwell et al., 2016). Thus, we first immunostained the 16 μm sections described above against podocalyxin (endothelial cell marker) and ASMA to assess vascular density. Briefly, tissues were washed in PBS and then permeabilised for 20 min with 3% triton-PBS before blocking with 5% donkey serum for 1 h. The tissues were then incubated overnight with 1:200 anti-podocalyxin antibody (AF1556, R&D Systems) and 1:50 anti-ASMA (ab5694, Abcam). After washing, anti-goat Alexa-647 (A21447, ThermoFisher), and anti-rabbit Alexa-488 (A10042, ThermoFisher) conjugated secondary antibodies were incubated 1:200 for 1 h at room temperature. Finally, the slides were mounted using mounting media containing DAPI (H1200, Vector Labs).

Images fitting the right and left ventral horn grey matter were analysed with ImageJ software by a blinded observer (S.A.L.). First, masks were created using a common threshold selection and then the "skeletonisation" function was used to measure the length of blood vessel structures as described previously (Lewandowski et al., 2016). Diameter of ASMA positive vessels was calculated dividing the total area of each continuous ASMA signal by their length. Each datapoint graphed is the average of at least 6 non-adjacent (~100 μm apart) tissue sections.

2.7. Motoneuron counts with Nissl staining

The same tissues described above were also used to assess motoneuron survival. Briefly, the tissues were first treated with a solution of 0.1% cresyl violet acetate for 20 min at 60 °C and then treated with increasing concentrations of ethanol. After a final treatment with HistoClear (HS200, National Diagnostics) the slides were mounted with DPX. Nissl-stained motoneurons were

counted every third section of the ventral horn region following previously published methods (Coughlan et al., 2015) (cell bodies between 30 and 80 μm in diameter, presence of a dark nucleolus and multi-polar structure) in 30-40 sections per animal.

2.8. huANG uptake by the spinal cord

WT (n = 3) and SOD1G93A (n = 2) mice were injected i.p. with 1 μg of huANG, sacrificed 2 h later (moment of peak huANG serum levels) and spinal cords taken and processed as described here previously. huANG was detected using human-specific antibodies that do not detect mouse angiogenin (Kishimoto et al., 2005). The lumbar spinal cord sections were immunostained using the same protocol described above, in this case against huANG (2.5 μg/mL, AF265, R&D Systems and 10 μg/mL, 26-2F, Millipore), glial fibrillary acidic protein (GFAP; 1:800, G9269, Sigma), ASMA (1:50, ab5694, Abcam) and podocalyxin (1:200, AF1556, R&D Systems) in order to assess huANG cellular uptake.

2.9. Statistical analysis

Non-survival graphs present the data as mean ± SEM. Differences in the means between two groups were analysed with t-tests when comparing two groups and ANOVA (post-hoc: Tukey's HSD test for unequal numbers) was used when analysing more than two groups. Survival curves were analysed with the log-rank test. Normality was assessed with the Shapiro-Wilks test and homoscedasticity with the Levene test.

3. Results

3.1. huANG levels are elevated in serum after systemic i.p. administration

Before commencing a more detailed preclinical study, we investigated serum levels and tissue distribution of huANG protein after i.p. administration to WT and SOD1^{G93A}. For pharmacokinetic studies, WT and SOD1^{G93A} mice were administered with 1 μg huANG or vehicle via i.p. injection at PND 90. Mice were sacrificed immediately after i.p. injection and at 2 h and 24 h, and peripheral blood samples were taken for serum collection and analysis. ELISA analysis (Fig. 2) showed that huANG serum levels peaked 2 h after i.p. injection (WT = 3106 ± 277 pg/mL; SOD1^{G93A} = 3688 ± 428 pg/mL) and were still elevated 24 h later (WT = 1330 ± 251 pg/mL; SOD1^{G93A} = 1738 ± 550 pg/mL). No significant differences were found between genotypes.

3.2. **huANG** *is taken up by astroglia and endothelia after systemic administration*

Previous work by our lab showed endogenous ANG to be expressed in the motoneurons of spinal cord sections in both WT and SOD1^{G93A} mice (Sebastià et al., 2009). In the present study, immunohistochemical analysis of ventral lumbar spinal cord sections revealed that exogenous huANG localized in the cytoplasm of astrocytes (as assessed by GFAP staining) and endothelial cells from grey and white matter 2 h after i.p. injection (time of peak serum concentration; Fig. 3a), with similar results for SOD1^{G93A} and WT mice. Other than their cell bodies, astrocyte projections around blood vessels were also positive for huANG, which could suggest direct uptake of huANG from endothelial cells into astrocytes (Fig. 3c). In contrast, we did not detect the presence of huANG in ASMA-positive cells, indicative of pericytes and SMCs, at the timepoint analysed (see Supplementary material 5). Vehicle-treated control animals did not show huANG staining in the spinal cord (Fig. 3b and d).

Mild huANG uptake was also detected in spinal cord astrocytes (in 4 out of 5 animals tested) at PND 115 after chronic administration of huANG followed by a 24-h 'wash out' period (Supplementary material 6), taken from the same batch of samples used in sections 3.4 and 3.5, and described in Fig. 1a. In contrast, we did not detect huANG in endothelial cells from these same spinal cord samples.

3.3. Systemic huANG administration delays motor dysfunction and improves survival of SOD1^{G93A} mice in a preclinical study paradigm

To explore the effect of chronic huANG administration on motor function and survival in a pre-clinical study design, huANG and vehicle (PBS) were administered via i.p. injections 3 times a week to sex- and litter-matched WT and SOD1^{G93A} mice. A marked decline in rotarod latency, ie. the time it took for each mouse to fall from the rotor at constant acceleration, was observed in vehicle-treated SOD1^{G93A} mice from PND 118 onward. In contrast, motor function skills declined later, from PND 139 onward, in huANG-treated mice. We observed statistically significant higher latencies to fall in huANG-treated SOD1^{G93A} compared to their vehicle-treated counterparts between PND 118 and 145 (Fig. 4; $p < 0.05$). Survival during this period was still at 100% for vehicle- and huANG-treated mice. As expected, WT mice motor skills were unchanged throughout the experiment, irrespective of treatment.

Survival of animals as assessed by Kaplan-Meier analysis revealed that huANG-treated SOD1^{G93A} mice had a significantly enhanced survival compared to vehicle-treated counterparts (Fig. 5a; Mantel-Cox test: $p < 0.01$). We also found this to be true for both male and female SOD1^{G93A} mice when analysed separately (Mantel-Cox test: $p < 0.02$; Fig. 5b and c).

3.4. huANG treatment protects against motoneuron loss

Previous data by our lab had shown huANG to extend motoneuron survival *in vitro* (Kieran et al., 2008; Sebastià et al., 2009). Analysis of motoneuron counts per ventral horn after Nissl staining demonstrated a significant decrease in the number of motoneurons in vehicle-treated SOD1^{G93A} mice compared to all groups (Fig. 6b; 2-way ANOVA, interaction: $p = 0.005$, post-hoc Tukey: $p < 0.05$). Of note, while being significantly higher than their vehicle-treated counterparts, motoneuron numbers in huANG-treated SOD1^{G93A} mice were significantly lower than vehicle-treated WT mice at the time point analysed (PND 115) but not significantly different from huANG-treated WT mice.

3.5. huANG treatment protects from vascular network regression

Previous studies detected endothelial damage before obvious symptomatology in SOD1 mutant mice, including reduced *ang* and *vascular endothelial growth factor* (*VEGF*) mRNA levels (Lu et al., 2007; Nardo et al., 2013; Zhong et al., 2008). Detection of huANG uptake into endothelial cells indeed suggests a potential effect on vascularization (Fig. 3b). We next immunostained the lumbar sections extracted from chronic huANG-treated mice against podocalyxin, an endothelial cell marker. Total blood vessel length corresponding to ventral horn grey matter area was then quantified as a metric of vascular health. We found that SOD1^{G93A} mice had reduced average vascular length per mm2 compared to their WT counterparts irrespective of treatment (Fig. 7b; 2-way ANOVA, interaction: ns, main effect genotype: $p < 0.05$). More interestingly, we observed huANG-treated mice had increased

vascular coverage compared to non-treated mice (Fig. 7b; 2-way ANOVA, interaction: ns, main effect treatment: $p < 0.01$). These results suggest there was significant vascular protection in huANG-treated $SOD1^{G93A}$ mice.

In contrast, we found no differences in total ASMA-positive vessel length per mm^2 of ventral horn grey matter area between any of the groups or in the percentage of ASMA-positive vessel length per total vessel length (see Supplementary material 7). However, we did detect a significant increase in the diameter of ASMA-positive blood vessel sections in $SOD1^{G93A}$ mice, irrespective of treatment (Fig. 8b. 2-way ANOVA, interaction: ns, main effect genotype: $p < 0.05$).

4. Discussion

Here we demonstrated that systemic huANG protein delivery post symptom onset extended survival, delayed motor dysfunction and protected against motoneuron loss. We observed huANG treatment to protect against vascular regression in $SOD1^{G93A}$ mice and the drug to be incorporated into astrocytes and endothelial cells, suggesting that huANG may act on multiple cell types to mediate potential therapeutic benefits.

In order to characterise serum levels and tissue uptake after systemic huANG delivery in our pre-clinical study, we initially measured the pharmacokinetics achieved by a 1 μg i.p. injection (Fig. 2) and found a marked increase of huANG serum levels 2 h post-injection in $SOD1^{G93A}$ and WT mice. huANG serum levels were reduced but remained detectable after 24 h. Very moderately elevated serum huANG levels have been previously reported in ALS but not Parkinson's disease patients (Cronin et al., 2006; van Es et al., 2014), suggesting that this may represent an endogenous stress response in ALS. These are interesting findings in the context of a previous *in vivo* study that demonstrated elevated *ang* expression in motoneurons micro-dissected from slowly progressing $SOD1^{G93A}$ mice after disease onset (Nardo et al., 2013). Intriguingly, those *ang* expression results were not found in a model of fast progressing $SOD1^{G93A}$ mice by the same authors. Further studies are required to determine whether ANG protein is secreted from motoneurons or depleted *in vivo* during disease progression, but the above results suggest exogenous huANG administration may represent a feasible strategy to boost stress responses in ALS.

The present study validates our previous report showing systemic huANG delivery prolongs survival, delays disease progression and protects motoneurons from degeneration *in vivo* (Kieran et al., 2008). Interestingly, vehicle-treated $SOD1^{G93A}$ mice featured a statistically significant loss of motoneurons (Fig. 6b), accompanied by a concomitant reduction in vascular coverage (Fig. 7b) in the ventral horn of the lumbar spinal cord. These defects were significantly countered in huANG-treated $SOD1^{G93A}$ mice, albeit not completely, suggesting our treatment paradigm supported motoneurons to cope with the disease burden rather than preventing or reversing it completely. These findings are of note in the context of previous studies that showed reductions in capillary length and endothelial tight-junctions already prior to disease onset and a correlation between reduced vascular network and survival in the $SOD1^{G93A}$ mouse model (Lewandowski et al., 2016; Zhong et al., 2008). Hence, the reduced motoneuron loss we observed in huANG-treated $SOD1^{G93A}$ mice could be explained, at least in part, by the safeguarding of blood flow to the cells.

We found significantly enhanced survival (Fig. 5) and delayed motor dysfunction (as measured by the rotarod test; Fig. 4) in huANG-treated SOD1^{G93A} mice. Motor-skills rated higher in huANG-treated SOD1^{G93A} between PND 118 to 145, after which point the treatment as designed here was no longer enough to differentiate motor function between treated and non-treated SOD1^{G93A} mice. The significant delay in motor dysfunction was found to start around the age point we found increased vascular coverage in treated SOD1^{G93A} mice (PND 115) and thus could also be linked to the angiogenic effects of huANG. Interestingly, the present immunohistochemical analysis showed exogenous huANG to localize in endothelial cells and astroglia after acute administration in WT and SOD1^{G93A} mice (Fig. 3). While ANG action on the endothelium is better understood, we have previously shown that huANG uptake into astrocytes contributes to motoneuron protection *in vitro* (Skorupa et al., 2012), suggesting that ANG activates multiple protective mechanisms when delivered systemically.

In this context, we have previously shown huANG treatment to change the profile of extracellular matrix components and enzymes secreted by astrocytes (Skorupa et al., 2013), including the upregulation of urokinase secretion, which can induce positive recovery effects after spinal cord injury *in vivo* and ischemic conditions on cortical neurons *in vitro* (Seeds et al., 2011; Wu et al., 2014). It is therefore possible astroglial secretions could mediate neuroprotection both directly and also indirectly by preventing vascular regression in response to ANG.

ANG induces endothelial cell growth by stimulating rDNA transcription (Hu et al., 2000; Sheng et al., 2014), a process that is required for the activity of angiogenic factors such as VEGF (Kishimoto et al., 2005). ANG can also bind cell-surface actin to induce the degradation of the endothelial basement membrane, thus allowing for vascular expansion (Hu et al., 1994). Additionally, ANG has pro-survival effects in mammalian cells by generating tRNA-derived, stress-induced small RNAs (tiRNAs) under certain stress conditions, such as hypoxia or nutrient starvation (Fu et al., 2009). tiRNAs inhibit translation, induce stress granule (SG) formation (Emara et al., 2010; Yamasaki et al., 2009) and can inhibit apoptosis by competitive binding of cytochrome c (Saikia et al., 2014). Results by our lab and others have also shown that ANG can affect motoneuron survival directly *in vitro*, i.e. when there is no possible interaction with glia or vasculature (Kieran et al., 2008; Sebastià et al., 2009). This means that apart from direct stimulation of endothelial cells and astrocytes, ANG could also contribute to motoneuron survival by other pathways such as the induction of tiRNAs.

Regional blood flow is regulated by contractile, ASMA-expressing cells, pericytes in capillaries and vascular SMCs in precapillary arterioles (Attwell et al., 2016). SOD1^{G93A} mice had an increased average contractile cell diameter irrespective of treatment (Fig. 8b), while we found no differences in ASMA + vessel coverage between the two genotypes analysed (Supplementary material 7). Pericyte and SMC dilation has been linked to prostaglandin EP4 receptor activation and nitric oxide (NO) respectively (Denninger and Marletta, 1999; Hall et al., 2014), the latter being a molecule reported to be synthesized and released by endothelial cells in response to ANG (Trouillon et al., 2010). There could be different factors interacting to explain our results. The observed vascular dilation in the case of untreated SOD1^{G93A} could be a compensatory mechanism in response to reductions in vascular network coverage, while the fact that huANG-treated SOD1^{G93A} mice also present increased dilation

could be a consequence of increased NO synthesis. At the same time, the lack of significant dilation in huANG-treated WT mice could imply that endothelial cells are somehow primed to synthesize NO in $SOD1^{G93A}$ mice compared to their WT counterparts.

5. Conclusions

Collectively, our results show the potential of ANG as a novel therapeutic with pleiotropic mechanisms of action on motoneuron survival and vascular health by acting on different cell types. We present evidence here to suggest exogenous huANG is acting directly on astrocytes and endothelial cells to mediate vascular growth and maintenance. Hence, ANG could present a new class of pleiotropic agents and candidates for future ALS therapeutics development.

Ethics approval and consent to participate

This study was conducted in strict accordance with Directive 2010/63/EU on the protection of animals used for scientific purposes. Ethical approval for the animal experiments carried out on this study was awarded by the Animal Research Ethics Committee of the Royal College of Surgeons in Ireland. Ethics reference number: REC1122b.

Conflicts of interest

J.H.M.P. is a beneficiary of patents relating to the use of angiogenin for the treatment of CNS diseases.

Authors' contributions

J.H.M.P. designed research; M.C., S.L.O'R., S.C., L.H., K.S.C., M.C.H. performed research; M.C., I.W., S.A.L., J.H.M.P analysed data; M.C. and J.H.M.P wrote the article.

Funding

J.H.M.P. is supported by an Enterprise Ireland Commercialisation Fund co-funded by the European Union (TD20090107) and a grant from the Health Research Board (HRA_POR/2013/348). S.A.L. is supported by Olle Engkvist Byggmästare Foundation (SLS-499431), Swedish FTD Initiative and Björklund Fund from Swedish Society of Medicine (SLS-499431).

References

Attwell, D., Mishra, A., Hall, C.N., O'Farrell, F.M., Dalkara, T., 2016. What is a pericyte? J Cereb Blood Flow Metab. 36, 451–455. doi:10.1177/0271678X15610340

Coughlan, K.S., Mitchem, M.R., Hogg, M.C., Prehn, J.H.M., 2015. "Preconditioning" with latrepirdine , an adenosine 5'-monophosphate-activated protein kinase activator, delays amyotrophic lateral sclerosis progression in SOD1 G93A mice. Neurobiol Aging. 36, 1140–1150. doi:10.1016/j.neurobiolaging.2014.09.022

Cronin, S., Greenway, M.J., Ennis, S., Kieran, D., Green, A., Prehn, J.H.M., Hardiman, O., 2006. Elevated serum angiogenin levels in ALS. Neurology. 67, 1833–1836. doi:10.1212/01.wnl.0000244466.46020.47

Denninger, J.W., Marletta, M. a., 1999. Guanylate cyclase and the NO/cGMP signaling pathway. Biochim Biophys Acta. 1411, 334–350. doi:10.1016/S0005-2728(99)00024-9

Emara, M.M., Ivanov, P., Hickman, T., Dawra, N., Tisdale, S., Kedersha, N., Hu, G., Anderson, P., 2010. Angiogenin-induced tRNA-derived stress-induced RNAs promote stress-induced stress granule assembly. J Biol Chem. 285, 10959–10968. doi:10.1074/jbc.M109.077560

Fett, J.W., Strydom, D.J., Lobb, R.R., Alderman, E.M., Bethune, J.L., Riordan, J.F., Vallee, B.L., 1985. Isolation and characterization of angiogenin, an angiogenic protein from human carcinoma cells. Biochemistry. 24, 5480–6. doi:10.1021/bi00341a030

Fu, H., Feng, J., Liu, Q., Sun, F., Tie, Y., Zhu, J., Xing, R., Sun, Z., Zheng, X., 2009. Stress induces tRNA cleavage by angiogenin in mammalian cells. FEBS Lett. 583, 437–442. doi:10.1016/j.febslet.2008.12.043

Greenway, M.J., Andersen, P.M., Russ, C., Ennis, S., Cashman, S., Donaghy, C., Patterson, V., Swingler, R., Kieran, D., Prehn, J.H.M., Morrison, K.E., Green, A., Acharya, K.R., Brown, R.H., Hardiman, O., 2006. ANG mutations segregate with familial and "sporadic" amyotrophic lateral sclerosis. Nat Genet. 38, 411–413. doi:10.1038/ng1742

Gurney, M.E., Pu, H., Chiu, A.Y., Dal Canto, M.C., Polchow, C.Y., Alexander, D.D., Caliendo, J., Hentati, A., Kwon, Y.W., Deng, H.X., Et, A., 1994. Motor neuron degeneration in mice that express a human Cu,Zn superoxide dismutase mutation. Science. 264, 1772–5. doi:10.1126/science.8209258

Hall, C.N., Reynell, C., Gesslein, B., Hamilton, N.B., Mishra, A., Sutherland, B.A., O'Farrell, F.M., Buchan, A.M., Lauritzen, M., Attwell, D., 2014. Capillary pericytes regulate cerebral blood flow in health and disease. Nature. 508, 55–60. doi:10.1038/nature13165

Hu, G., Riordan, J.F., Vallee, B.L., 1994. Angiogenin promotes invasiveness of cultured endothelial cells by stimulation of cell-associated proteolytic activities. Proc Natl Acad Sci U S A. 91, 12096–12100. doi:10.1073/pnas.91.25.12096

Hu, G., Xu, C.J., Riordan, J.F., 2000. Human angiogenin is rapidly translocated to the nucleus of human umbilical vein endothelial cells and binds to DNA. J Cell Biochem. 76, 452–462. doi:10.1002/(SICI)1097-4644(20000301)76:3<452::AID-JCB12>3.0.CO;2-Z

Kieran, D., Sebastià, J., Greenway, M.J., King, M.A., Connaughton, D., Concannon, C.G., Fenner, B., Hardiman, O., Prehn, J.H.M., 2008. Control of motoneuron survival by angiogenin. J Neurosci. 28, 14056–14061. doi:10.1523/jneurosci.3399-08.2008

Kishimoto, K., Liu, S., Tsuji, T., Olson, K.A., Hu, G., 2005. Endogenous angiogenin in endothelial cells is a general requirement for cell proliferation and angiogenesis. Oncogene. 24, 445–56. doi:10.1038/sj.onc.1208223

Lewandowski, S.A., Nilsson, I., Fredriksson, L., Lonnerberg, P., Muhl, L., Zeitelhofer, M., Adzemovic, M.Z., Nichterwitz, S., Lawrence, D.A., Hedlund, E., Eriksson, U., 2016. Presymptomatic activation of the PDGF-CC pathway accelerates onset of ALS neurodegeneration. Acta Neuropathol. 131, 453–464. doi:10.1007/s00401-015-1520-2

Lu, L., Zheng, L., Viera, L., Suswam, E., Li, Y., Li, X., Estévez, a G., King, P.H., 2007. Mutant Cu/Zn-superoxide dismutase associated with amyotrophic lateral sclerosis destabilizes vascular endothelial growth factor mRNA and downregulates its expression. J Neurosci. 27, 7929–7938. doi:10.1523/JNEUROSCI.1877-07.2007

Ludolph, A.C., Bendotti, C., Blaugrund, E., Chio, A., Greensmith, L., Loeffler, J.-P., Mead, R., Niessen, H.G., Petri, S., Pradat, P.-F., Robberecht, W., Ruegg, M., Schwalenstöcker, B., Stiller, D., van den Berg, L.H., Vieira, F., von Horsten, S., 2010. Guidelines for preclinical animal research in ALS/MND: A consensus meeting. Amyotroph Lateral Scler. 11, 38–45. doi:10.3109/17482960903545334

Nardo, G., Iennaco, R., Fusi, N., Heath, P.R., Marino, M., Trolese, M.C., Ferraiuolo, L., Lawrence, N., Shaw, P.J., Bendotti, C., 2013. Transcriptomic indices of fast and slow disease progression in two mouse models of amyotrophic lateral sclerosis. Brain. 136, 3305–3332. doi:10.1093/brain/awt250

Robberecht, W., Philips, T., 2013. The changing scene of amyotrophic lateral sclerosis. Nat Rev Neurosci. 14, 1–17. doi:10.1038/nrn3430

Rosen, D.R., 1993. Mutations in Cu/Zn superoxide dismutase gene are associated with familial amyotrophic lateral sclerosis. Nature. 364, 362. doi:10.1038/364362c0

Rothstein, J.D., 2017. Edaravone: A new drug approved for ALS. Cell 171, 725. doi:10.1016/j.cell.2017.10.011

Saikia, M., Jobava, R., Parisien, M., Putnam, A., Krokowski, D., Gao, X.-H., Guan, B.-J., Yuan, Y., Jankowsky, E., Feng, Z., Hu, G., Pusztai-Carey, M., Gorla, M., Sepuri, N.B. V, Pan, T., Hatzoglou, M., 2014. Angiogenin-cleaved tRNA halves interact with cytochrome c, protecting cells from apoptosis during osmotic stress. Mol Cell Biol. 34, 2450–63. doi:10.1128/MCB.00136-14

Sebastià, J., Kieran, D., Breen, B., King, M.A., Netteland, D.F., Joyce, D., Fitzpatrick, S.F., Taylor, C.T., Prehn, J.H.M., 2009. Angiogenin protects motoneurons against hypoxic injury. Cell Death Differ. 16, 1238–1247. doi:10.1038/cdd.2009.52

Seeds, N., Mikesell, S., Vest, R., Bugge, T., Schaller, K., Minor, K., 2011. Plasminogen activator promotes recovery following spinal cord injury. Cell Mol Neurobiol. 31, 1–7. doi:10.1007/s10571-011-9701-6

Sheng, J., Yu, W., Gao, X., Xu, Z., Hu, G., 2014. Angiogenin stimulates ribosomal RNA transcription by epigenetic activation

of the ribosomal DNA promoter. J Cell Physiol. 229, 521–529. doi:10.1002/jcp.24477

Skorupa, A., King, M.A., Aparicio, I.M., Dussmann, H., Coughlan, K.S., Breen, B., Kieran, D., Concannon, C.G., Marin, P., Prehn, J.H.M., 2012. Motoneurons secrete angiogenin to induce RNA cleavage in astroglia. J Neurosci. 32, 5024–5038. doi:10.1523/JNEUROSCI.6366-11.2012

Skorupa, A., Urbach, S., Vigy, O., King, M.A., Chaumont-Dubel, S., Prehn, J.H.M., Marin, P., 2013. Angiogenin induces modifications in the astrocyte secretome: Relevance to amyotrophic lateral sclerosis. J Proteomics. 91, 274–285. doi:10.1016/j.jprot.2013.07.028

Trouillon, R., Kang, D.K., Park, H., Chang, S.I., Ohare, D., 2010. Angiogenin induces nitric oxide synthesis in endothelial cells through PI-3 and akt kinases. Biochemistry. 49, 3282–3288. doi:10.1021/bi902122w

Van Es, M.A., Schelhaas, H.J., Van Vught, P.W.J., Ticozzi, N., Andersen, P.M., Groen, E.J.N., Schulte, C., Blauw, H.M., Koppers, M., Diekstra, F.P., Fumoto, K., Leclerc, A.L., Keagle, P.J., Bloem, B.R., Scheffer, H., Van Nuenen, B.F.L., Van Blitterswijk, M., Van Rheenen, W., Wills, A.M., Lowe, P.P., Hu, G., Yu, W., Kishikawa, H., Wu, D., Folkerth, R.D., Mariani, C., Goldwurm, S., Pezzoli, G., Van Damme, P., Lemmens, R., Dahlberg, C., Birve, A., Fernández-Santiago, R., Waibel, S., Klein, C., Weber, M., Van Der Kooi, A.J., De Visser, M., Verbaan, D., Van Hilten, J.J., Heutink, P., Hennekam, E.A.M., Cuppen, E., Berg, D., Brown, R.H., Silani, V., Gasser, T., Ludolph, A.C., Robberecht, W., Ophoff, R.A., Veldink, J.H., Pasterkamp, R.J., De Bakker, P.I.W., Landers, J.E., Van De Warrenburg, B.P., Van Den Berg, L.H., 2011. Angiogenin variants in Parkinson disease and amyotrophic lateral sclerosis. Ann Neurol. 70, 964–973. doi:10.1002/ana.22611

van Es, M.A., Veldink, J.H., Schelhaas, H.J., Bloem, B.R., Sodaar, P., van Nuenen, B.F.L., Verbeek, M., van de Warrenburg, B.P., van den Berg, L.H., 2014. Serum angiogenin levels are elevated in ALS, but not Parkinson's disease. J Neurol Neurosurg Psychiatry. 85, 1439–40. doi:10.1136/jnnp-2013-307168

Wu, D., Yu, W., Kishikawa, H., Folkerth, R.D., Iafrate, A.J., Shen, Y., Xin, W., Sims, K., Hu, G., 2007. Angiogenin loss-of-function mutations in amyotrophic lateral sclerosis. Ann. Neurol. 62, 609–617. doi:10.1002/ana.21221

Wu, F., Catano, M., Echeverry, R., Torre, E., Haile, W.B., An, J., Chen, C., Cheng, L., Nicholson, A., Tong, F.C., Park, J., Yepes, M., 2014. Urokinase-type plasminogen activator promotes dendritic spine recovery and improves neurological outcome following ischemic stroke. J Neurosci. 34, 14219–32. doi:10.1523/JNEUROSCI.5309-13.2014

Yamasaki, S., Ivanov, P., Hu, G., Anderson, P., 2009. Angiogenin cleaves tRNA and promotes stress-induced translational repression. J Cell Biol. 185, 35–42. doi:10.1083/jcb.200811106

Zhong, Z., Deane, R., Ali, Z., Parisi, M., Shapovalov, Y., O'Banion, M.K., Stojanovic, K., Sagare, A.P., Boillee, S., Cleveland, D.W., Zlokovic, B. V, 2008. ALS-causing SOD1 mutants generate vascular changes prior to motor neuron degeneration. Nat Neurosci. 11, 420–422. doi:10.1038/nn2073

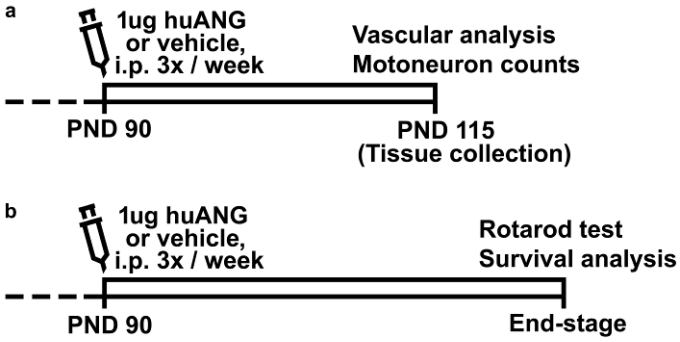

Fig. 1 Treatment design. Two groups of age- litter- and sex-matched WT and SOD1^{G93A} mice started treatment at day 90 of age, receiving 3 intra-peritoneal 1 µg huANG or vehicle (PBS) injections per week. **a** In order to assess how the vascular network and motoneuron numbers evolved, one group of mice had treatment terminated at day 115 of age and spinal cord tissue collected for Nissl staining and immunostaining against vascular markers (podocalyxin; ASMA). **b** A different group of mice was used for lifespan studies, assessing survival via Kaplan-Meier analysis and motorfunction via rotarod test through to disease end stage.

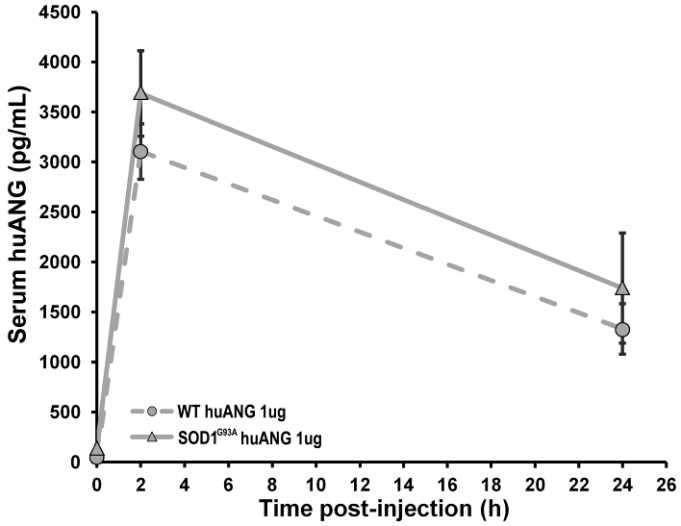

Fig. 2 No differences in pharmacokinetic response between WT and SOD1^{G93A} mice after 1 µg huANG injection. SOD1^{G93A} and WT littermates were injected with one acute i.p. dosage of 1 µg huANG protein and serum levels were determined by ELISA at 0h, 2h and 24h post-injection. Serum huANG peaked 2 h post-injection and was still detectable 24 h later, with no significant differences between genotypes. Each datapoint represents the mean +/- SEM. 0h WT n=6, SOD1^{G93A} n=6; 2h WT n=8, SOD1^{G93A} n=5; 24h WT n=7, SOD1^{G93A} n=6. t-test, WT vs SOD1^{G93A}, ns.

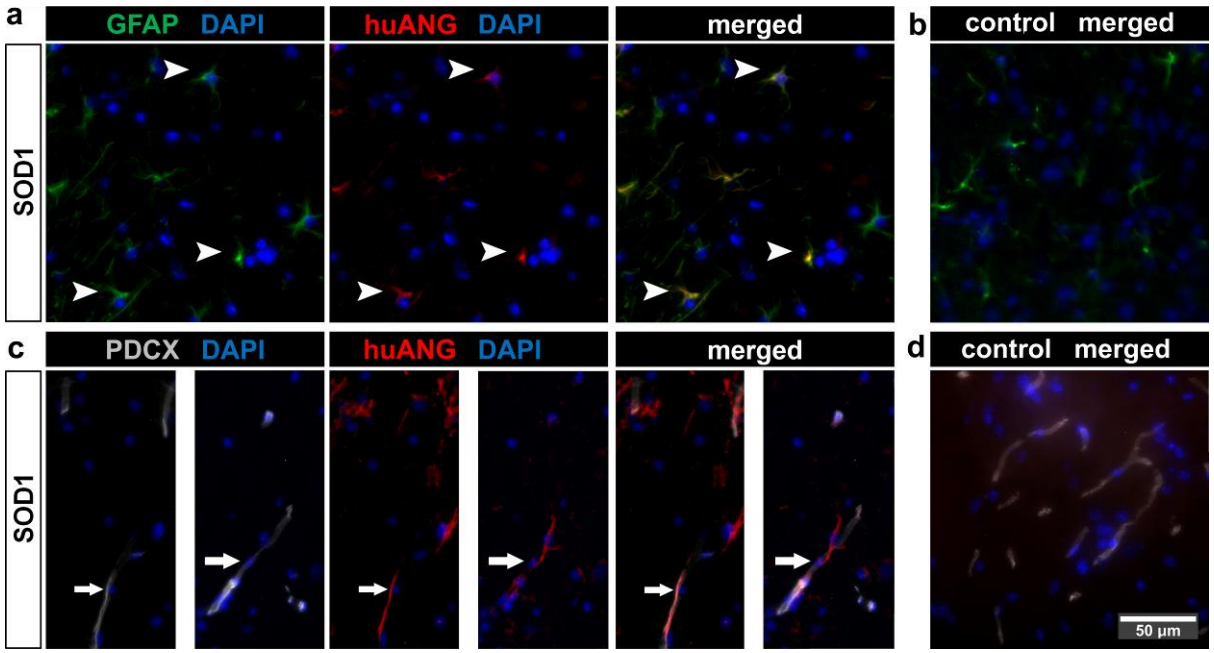

Fig. 3 huANG is taken up by astrocytes 2 hours after 1 µg huANG injection. SOD1^{G93A} and WT mice were injected with one acute i.p. dosage of 1 µg huANG protein at 90 days of age, and lumbar spinal cords removed for immunohistological analysis. **a** Representative image from ventral lumbar spinal cord sections from a SOD1^{G93A} mouse immunostained against huANG (red) and GFAP (green), with DAPI-stained nuclei in blue. Astrocytes, as detected by GFAP staining, can be seen to have incorporated huANG (white arrowheads). **b** Representative image from a control PBS-injected mouse. huANG (red) and GFAP (green), with DAPI-stained nuclei in blue. **c** Representative image from lumbar spinal cord sections from a SOD1^{G93A} mouse immunostained against huANG (red) and podocalyxin (white), with DAPI-stained nuclei in blue. Endothelial cells, as detected by podocalyxin staining, can be seen to have incorporated huANG, with huANG-positive astrocyte processes in contact with them (white arrows). **d** Representative image from a control PBS-injected mouse. huANG (red) and podocalyxin (white), with DAPI-stained nuclei in blue.

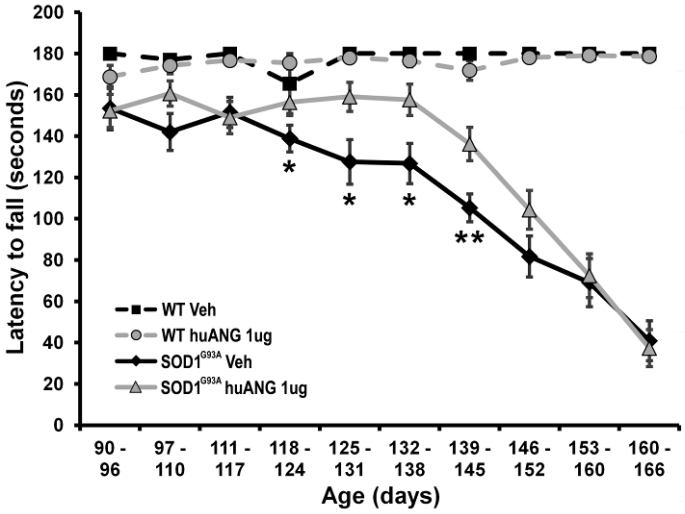

Fig. 4 huANG-treated SOD1^{G93A} mice perform better during the rotarod test versus non-treated counterparts. Mice from all groups were injected with 1 µg huANG or vehicle (PBS) three times a week and rotarod tested for a maximum of 180 seconds twice a week. Latency until fall from the rotarod was assessed up to three times and last value recorded. WT:huANG n=23; SOD1^{G93A}:huANG n=24; WT:VEH n=8; SOD1^{G93A}:VEH n=21. * t-test between SOD1^{G93A} groups, $p<0.05$ ** t-test between SOD1^{G93A} groups, $p<0.005$.

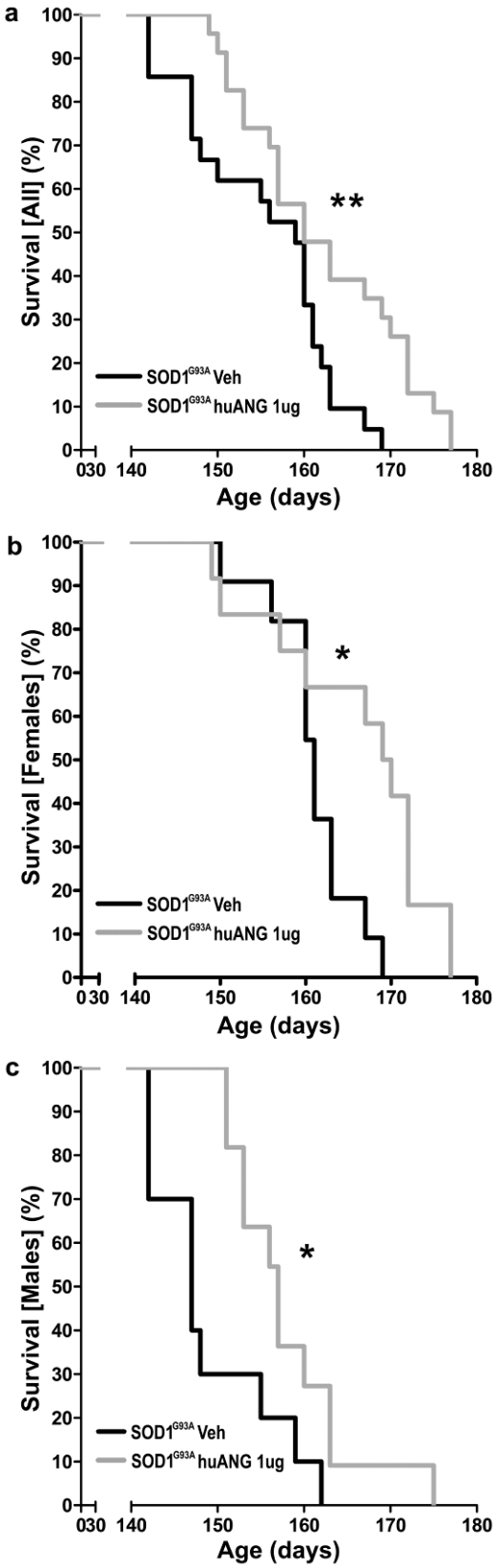

Fig. 5 huANG-treated SOD1^{G93A} mice showed increased survival compared to their vehicle-treated counterparts. Kaplan-Meier analysis of survival probabilities for huANG-treated (1 µg) and vehicle-treated (PBS) SOD1^{G93A} mice. **a** Gender balanced results. SOD1^{G93A}:VEH n=21, SOD1^{G93A}:huANG n=23. ** Mantel-Cox test: $p<0.01$ **b** Results from females only. SOD1^{G93A}:VEH n=11, SOD1^{G93A}:huANG n=12. * Mantel-Cox test: $p<0.05$ **c** Results from males only. SOD1^{G93A}:VEH n=10, SOD1^{G93A}:huANG n=11. * Mantel-Cox test, $p<0.05$.

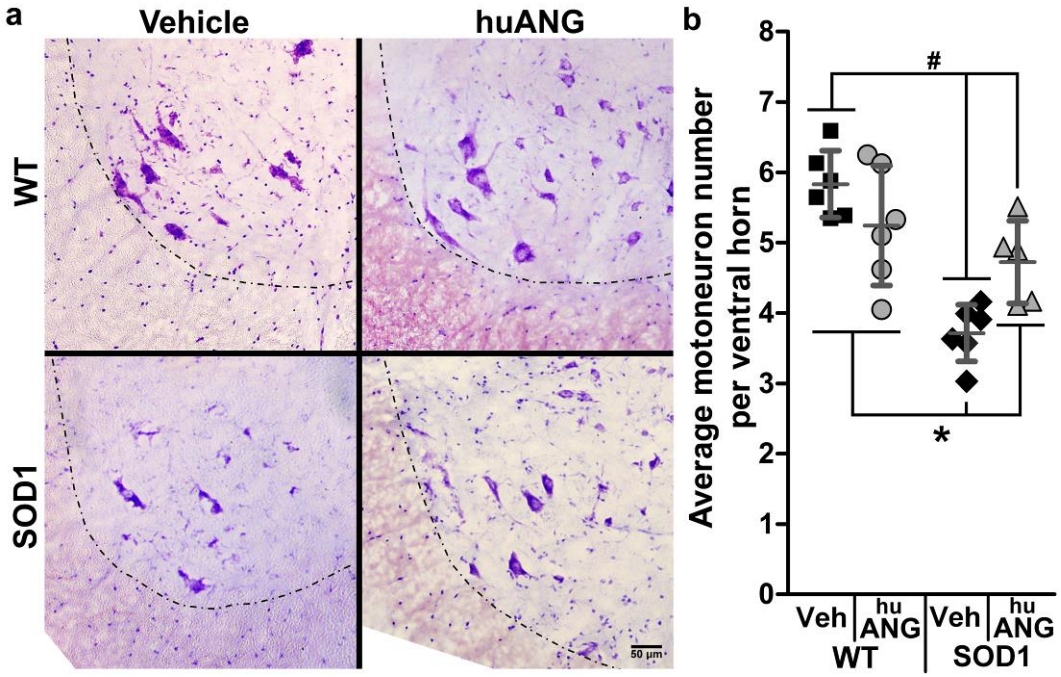

Fig. 6 Nissl staining showed huANG treatment prevented lumbar spinal cord motoneuron loss in SOD1^{G93A} mice. a Representative images from ventral horn area spinal cord tissue obtained at 115 days of age (25 days into treatment) from WT vehicle-treated mice (upper left panel), WT huANG-treated mice (upper right panel), SOD1^{G93A} vehicle-treated mice (lower left panel) and SOD1^{G93A} huANG-treated mice (lower right panel). Dashed line delimits grey and white matter area. **b** Average motoneuron numbers per ventral horn. Each datapoint represents mean motoneuron counts from 30-40 tissue slices along the lumbar spinal cord, dark grey lines represent mean +/- SEM. n=5-6. ***** Two-way ANOVA. Double interaction, treatment and genotype: p=0.005. Post-hoc: Tukey, SOD1^{G93A}:VEH vs all other groups: p<0.05. # Two-way ANOVA. Double interaction, treatment and genotype: p=0.005. Post-hoc: Tukey, SOD1^{G93A}:huANG vs SOD1^{G93A}:VEH and WT:VEH: p<0.05.

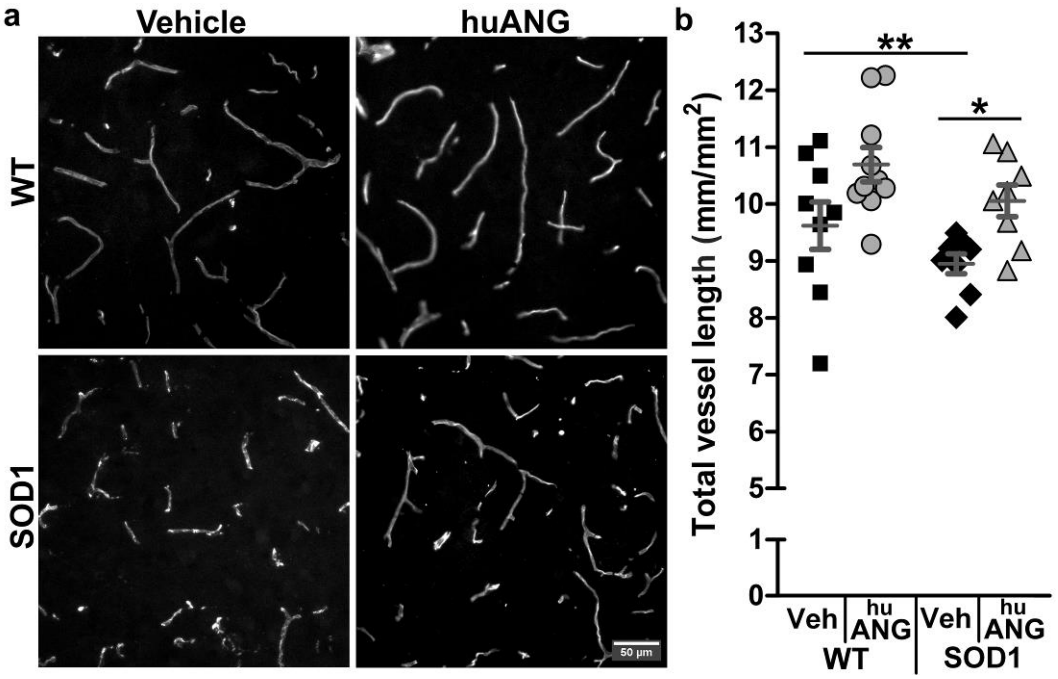

Fig. 7 huANG treatment protected spinal cord vascular network from regression as assessed by podocalyxin immunostaining. a Representative images from ventral horn grey-matter area from WT vehicle-treated mice (upper left panel), WT huANG-treated mice (upper right panel), $SOD1^{G93A}$ vehicle-treated mice (lower left panel) and $SOD1^{G93A}$ huANG-treated mice (lower right panel) at 115 days of age (25 days into treatment). **b** Total vessel length per area. Each datapoint represents mean values from 6, non-consecutive tissue slices from the lumbar spinal cord, dark grey lines represent mean +/- SEM. n=8-10. ***** Two-way ANOVA. Interaction, ns. Main effect: genotype: $p<0.05$ ****** Two-way ANOVA. Interaction, ns. Main effect: treatment: $p<0.002$.

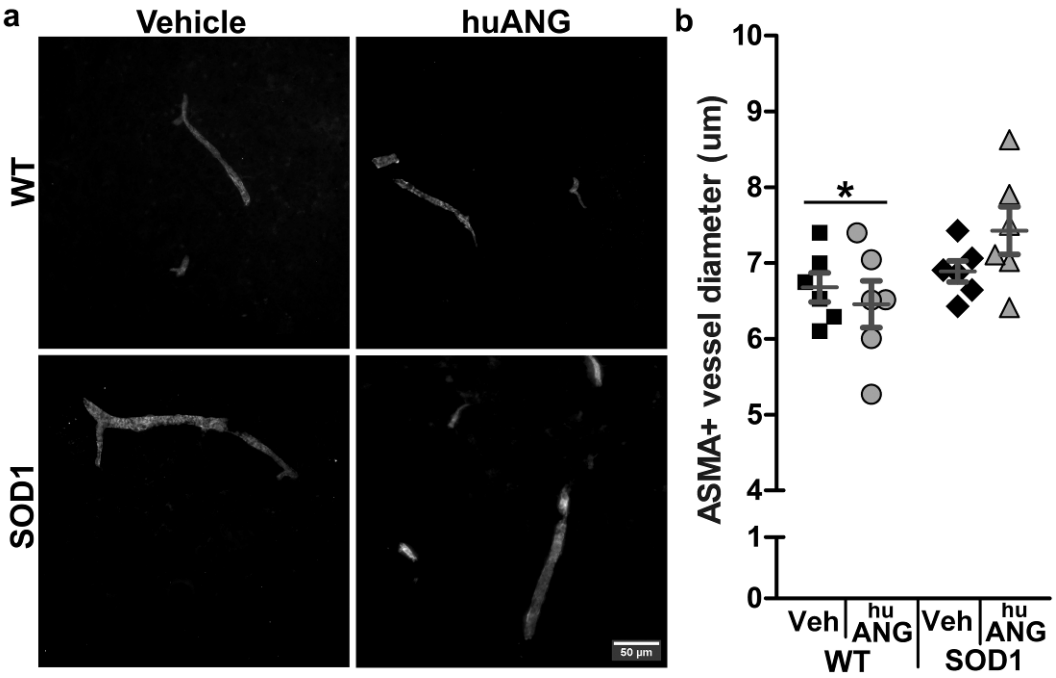

Fig. 8 ASMA immunostaining showed increased contractile vascular cell dilation irrespective of treatment in SOD1^{G93A} mice. a Representative images from ventral horn grey-matter area from WT vehicle-treated mice (upper left panel), WT huANG-treated mice (upper right panel), SOD1^{G93A} vehicle-treated mice (lower left panel) and SOD1^{G93A} huANG-treated mice (lower right panel) at 115 days of age (25 days into treatment). **b** Average diameter of ASMA-positive blood vessel sections quantified by dividing the area of each continuous ASMA-positive structure by its length. Each datapoint represents mean values from 6, non-consecutive tissue slices, dark grey lines represent mean +/- SEM. n=6. ***** Two-way ANOVA. Interaction, ns. Main effect: treatment: ns. Main effect: genotype: $p<0.05$.